Insights into the Arsenic Shell Decapping Mechanisms in As/GaAs Nanowires by X-ray and Electron Microscopy

Louise Fouquat, Xin Guan, Claude Botella, G. Grenet, Philippe Regreny, Michel Gendry, Hemian Yi, Jose Avila, Matthieu Bugnet, Jose Penuelas

Insights into the arsenic shell decapping mechanisms in As/GaAs nanowires by x-ray and electron microscopy

Louise Fouquat[1], Xin Guan[1], Claude Botella[1], Geneviève Grenet[1], Philippe Regreny[1], Michel Gendry[1], Hemian Yi[2], José Avila[2], Matthieu Bugnet[3*], José Penuelas[1**]

[1] Univ Lyon, Ecole Centrale de Lyon, CNRS, INSA Lyon, Université Claude Bernard Lyon 1, CPE Lyon, INL, UMR 5270, 69130 Ecully, France

[2] ANTARES Beamline, Synchrotron SOLEIL & Université Paris-Saclay, L'Orme des Merisiers, Gif sur Yvette Cedex, France

[3] Univ Lyon, CNRS, INSA Lyon, UCBL, MATEIS, UMR 5510, 69621 Villeurbanne, France

* To whom correspondence should be addressed. E-mail: matthieu.bugnet@insa-lyon.fr

** To whom correspondence should be addressed. E-mail: jose.penuelas@ec-lyon.fr

ABSTRACT:

Nanowire heterostructures of the oxide (shell) - semiconducting (core) type are of interest for various applications in energy harvesting, such as electrodes for photocatalysis, and in sensors. Their complete synthesis often requires the deposition of shell and core in two separate reactors, with the risk of exposing the core to oxidation from atmospheric conditions during transfer. Here, we study the desorption mechanisms and protection efficiency of an arsenic shell, which was purposely deposited on the GaAs core for protection against undesirable oxidation. Using *in situ* heating in the transmission electron microscope and synchrotron radiation scanning photoelectron microscopy, we explore the morphology, the structure and the surface chemistry of GaAs nanowires capped with an arsenic shell, from room temperature up to 500 ºC. A phase transformation from amorphous to polycrystalline arsenic is evidenced at a temperature about 300°C, alongside the disappearance of the surface oxidation observed at room temperature. At higher temperature, the arsenic shell desorbs with an activation energy of 2.32 eV, leading to clean facets. These results are helpful to determine pathways towards improving the efficiency of oxidation-protective layers on III-V semiconducting nanostructures.

KEYWORDS: III-V nanowires, core-shell, oxidation, annealing, *in situ* transmission electron microscopy, scanning photoelectron microscopy.

Introduction

III-V semiconducting nanowires (NWs) are promising for a large range of applications including solar energy harvesting [1-5], microelectronics [6] and integrated photonics [7-17]. In most of these applications, an epitaxial shell or a passivation layer wrapping the III-V core of the NW is needed to modify their functional properties or to avoid the formation of surface recombination traps due to undesirable oxidation. Materials such as silicon and germanium [18, 19], aluminum [20, 21], Fe_3Si [22] and $SrTiO_3$ [23] have been used as shell-material wrapping of III-V NWs to enhance or optimize their properties. Nevertheless, growing such heterogeneous shells is challenging; in most cases the shell and the core must be deposited in separate reactors, which implies that the oxidation of the as-deposited III-V facets must be avoided when the NWs are transferred between the deposition chambers. The strategy to avoid oxidation must preserve the quality of the NW facets from the point of view of their crystallography, their morphology and their surface chemistry. Besides the obvious use of connected ultra-high vacuum (UHV) reactors [21, 22], various methods have been suggested to obtain clean III-V facets for an epitaxial shell growth, such as for example cleaning by atomic hydrogen [24, 25]. Among them, the reversible capping by arsenic [26] presents several advantages. Firstly, As can be one of the constitutive element of III-V semiconductors, *e.g.*, in GaAs or InAs, and consequently this approach does not require the introduction of any additional element, which could modify the nature of the surfaces. Secondly, the As decapping is obtained through heating at rather moderate temperature (less than 400°C), and can be performed in standard growth reactors or *in situ* in scanning tunneling microscopes (STM) [27-31]. Despite its practical importance, the physical mechanism behind the NW decapping has not been much studied, except by reflective high energy electron diffraction (RHEED) and x-ray photoelectron spectroscopy (XPS) [26], and STM [30]. It has been shown that even if the capping protects the NW facets well enough for subsequent epitaxial shell growth, it may

induce surface defects that require nanometer resolution analysis on a single NW, such as transmission electron microscopy (TEM), compared to characterization techniques operating at larger scales such as RHEED and XPS, which intrinsically probe a NW assembly. Therefore, the objective of this work is to combine thermal annealing using *in situ* TEM, and scanning photoelectron microscopy (SPEM) to determine how the morphology, the structure, and the surface chemistry evolve during the decapping of an As shell wrapping a single GaAs NW.

Results and Discussion

The RHEED pattern obtained after the growth of GaAs NWs of sample S1 (see experimental section) and shown in Figure 1(a) indicates that the epitaxial growth axis of the NWs, i.e., perpendicular to the surface of the substrate, is [111], confirming our previous observations [**26**]. The RHEED pattern exhibits spots related to both Zinc-Blende (ZB) and Wurtzite (WZ) phases, as described elsewhere [**32, 33**]. After the As capping, the RHEED pattern shown in Figure 1(b) does not exhibit spots related to GaAs, in agreement with the presence of an amorphous As shell that completely covers the GaAs NWs and hinders the RHEED signal from the core. The NWs are vertical with an approximate length of 1.7 µm and a density of about 4 NWs/µm^2, as shown in the scanning electron microscopy (SEM) image of the As-capped sample S1 in Figure 1(c). These NWs are well separated and do not shadow each other, which is crucial to obtain a uniform and conformal As shell using MBE. Nearly all the As-capped GaAs NWs of sample S1 have a uniform core diameter of 80 nm. The NWs of sample S2 exhibit a similar structure with a core diameter of about 150 nm and a length of about 9.0 µm.

The As-capped GaAs NWs were ripped from their native substrate. For TEM observations, sample S1 was deposited onto a micro-electro-mechanical system (MEMS) DENSsolutions

Wildfire chip, optimized for *in situ* annealing within the TEM column. For SPEM and XPS measurements, sample S2 was deposited on a Si substrate with its native oxide removed.

The bright field TEM image and elemental maps shown in Figure 2 confirm the core-shell NW structure with a core diameter of about 80 nm, and a conformal and smooth amorphous As shell of about 40 nm thickness. The Ga droplet at the NW tip is not visible due to its exposure to As atmosphere, which induced the formation of a crystalline WZ GaAs segment of about 150 nm length. The origin of this ZB / WZ transition has been thoroughly discussed [**32, 34, 35**], and is thought to be resulting from the evolution of the Ga droplet contact angle during the growth [**36-39**].

After NW dispersion onto Si substrate, sample S2 was rapidly sealed into the UHV chamber of the ANTARES beamline at synchrotron SOLEIL [**40**]. It should be noted that SPEM experiments could also be performed on vertical NW grown on their original substrate [**41, 42**], however we dispersed the NWs on a substrate in order to measure individual NWs. Figure 3(a) shows the XPS spectrum of sample S2 acquired with a large spot size. Only the As 3*d* core levels are visible; the Ga 3*d* photoelectrons cannot escape the shell thickness because of their shorter mean free path. The position of the As $3d_{5/2}$ core level at about 41.4 eV is that of metallic As. The spin orbit splitting is clearly evidenced. Oxidation of the exposed As shell is also detected in small quantity at about 44.4 eV due to the exposition to air prior to insertion into the XPS chamber. However, the prevalence of metallic As attests of the efficiency of the shell protective role. The beam was then focused by means of Fresnel zone plates in order to obtain a pixel size of about 400×400 nm². The SPEM image of Figure 3(b) shows that the NWs are well distributed on the surface and have the expected length. It should be noted that because the expected NW diameters (about 230 nm) are smaller than the pixel size, the NW diameter is overestimated in SPEM images. A series of four As 3*d* spectra have been extracted along the length of a single NW, in addition to one spectrum from the substrate as reference (Figure 3(c)).

The four spectra from the NW are similar (the doublet structure of the As *3d* peak is well resolved and the As oxide is alike) and therefore demonstrate the NW homogeneity. Comparable measurements have been obtained on several NWs.

For *in situ* TEM annealing of sample S1, the temperature of the SiN_x membrane supporting the dispersed NWs was directly increased to 200 ºC, and then incrementally stepped by 5 °C every 30 s, up to 380°C. It should be mentioned that upon annealing, the structural evolution of GaAs NWs was observed to occur only in some NWs, while other NWs would undergo the same structural transformation after the temperature is raised tens or hundreds of degrees higher. It is thus apparent that the structural evolution of the NWs varies strongly as a function of the nature of the thermal contact between the nanowires and the SiN_x membrane, which depends on various factors like the NW bending, important here for NWs as long as 1.7 µm, and the NW interface with the supporting membrane (*e.g.*, presence of amorphous hydrocarbon species at the NW surface, oxidation of the NW facets, presence of defects like atomic steps, etc.). The decapping process on NWs grown in the same conditions as sample S1 was also performed in the MBE chamber, and followed by RHEED. The *in situ* TEM results reported in this manuscript show structural and chemical modifications of NWs where the temperature of the SiN_x membrane, which is accurately measured directly by the 4-point probe DENSSolutions system in the TEM [43, 44], is in agreement with the temperature measured during decapping in the MBE chamber.

Above 300 °C, the NW surface became rough, as the amorphous As shell turns polycrystalline (see Supporting Information Figure S1). This crystallization was previously reported to occur at 306 °C in thick layers of amorphous As by differential thermal analysis [45], in good agreement with our observations. The homogeneous crystallization over the length of this NW suggests that it is lying flat on the SiN_x membrane, providing a homogeneous thermal contact.

This is different from the NW shown in Video V1 (see Supporting Information), where the slow progression of the crystallization front from top to bottom suggests that the thermal contact with the membrane is better at the top of the NW. While the crystallization of the NW in Video V1 seems to start from the outer part of the As shell, especially on the top left of the NW, which could be attributed to the fact that it constitutes a free surface, additional evidence should be provided to support this hypothesis. At around 310 °C, the crystalline As shell begins to disappear (Figure 4). At around 365 °C, the As shell is not visible anymore and the GaAs surface is clean and smooth. Recently, *in situ* heating experiments in the TEM have been realized to estimate activation energies of various phenomena in III-V NWs, such as GaAs replacement by Au [**46, 47**] or defect dynamics [**48**]. The same method has been applied here to extract the activation energy of the present As desorption mechanism. From 300 to 380 °C, the diameter D of the NW was measured in order to calculate the corresponding arsenic desorption velocity k (see Supporting Information for details concerning the data measurement). This desorption velocity can be related to an activation energy E_a (see Figure 4b) equal to 2.32 eV, a value slightly smaller than the cohesive energy of As, which varies from E_c = 2.4 eV per As atom to E_c = 3.0 eV per As atom depending on the crystalline phase [**49**]).

Figure 5 shows the As 3*d* core level photoemission spectra measured on sample S2 before annealing, after a first annealing (30 min) at 400°C, and after a second annealing (30 min) at 440°C. It should be noted that this temperature is probably overestimated compared to the temperature measured during MBE growth. After the first annealing, the XPS spectrum does not display Ga 3*d* core level (see Figure S3), which means that the As capping is still wrapping the NWs. However, the As 3*d* core level does not exhibit As oxide (grey-filled area) anymore. After the second annealing at 440°C, the As 3*d* core levels are strongly modified. A shift toward low binding energy is clearly evidenced, and a broadening is observed. This energy shift agrees well with a modification of the As environment from As-As to Ga-As, as expected after As

shell desorption. The broadening of the As 3*d* peaks could be the consequence of residual As at the surface and/or surface defects. The fitting parameters are available in Supporting Information (Table S1).

Elemental maps extracted from EELS data after the *in situ* decapping in the TEM indicate the complete desorption of the As shell, as illustrated in Figure 6. Spectra on the nanowire show both Ga L_{23} and As L_{23} contributions at ~1120 eV and ~1330 eV, respectively, as shown in Figure S4. The O-K edge at ~530 eV is not detected on the NW, suggesting that the As shell protects the nanowire from oxidation. This is in good agreement with the As 3*d* core level XPS spectra (Figure 5(c)), which indicate a GaAs surface without traces of oxidation. However, the As 3*d* peaks are broad, which could be explained by the presence of surface defects such as As_{Ga} antisite defects as observed by STM [30]). Moreover, the high resolution TEM image in Figure 6 shows that the NW surface is crystalline, and strongly facetted, comparable to as grown NWs, opening the way for further epitaxial growth. These results can be compared with NWs that have been exposed to air, and which exhibit a thin amorphous oxide shell [26].

Conclusions

In summary, we combined *in situ* heating of core(GaAs)-shell(As) NWs in the TEM and synchrotron radiation scanning photoemission microscopy to explore the structural changes of GaAs nanowires capped with an As shell upon annealing, which is a conventional step towards the growth of oxide shells on III-V cores in NW geometry. The results unambiguously show that the As decapping is preceded by the crystallization of the initially amorphous As shell at ~300 ºC. Beyond this temperature, the arsenic shell desorbs with an activation energy of ~2.32 eV, leading to clean facets of the NW core, which supports the success of this approach to promote the subsequent epitaxial growth of an oxide shell. Two desorption phenomena were

identified, which could correspond to As oxide desorption and metallic As desorption. This work demonstrates that the capping / decapping process is efficient to obtain clean GaAs nanowires surfaces (stable until 600 °C [50]), and could be suitable for other arsenide NWs such as InAs (stable until 380 °C [51]). The proposed method allows to obtain clean facets in the high vacuum of a TEM column, and UHV setups equipped with a heater, thus opening the way to surface science studies on arsenide NWs.

Experimental Section

Nanowire Synthesis

Self-catalyzed GaAs NWs were grown on epiready Si(111) substrates by molecular beam epitaxy (MBE). The substrates were cleaned with ethanol and acetone for 5 min in order to remove surface contaminations. After rinsing, the substrates were outgassed at 200°C under UHV for a few minutes and then transferred into the MBE chamber. The MBE chamber is equipped with a Ga Knudsen cell with an incident angle of 27.9° [*52*] and an As valve cracked cell. GaAs NWs were grown using the VLS mechanism with Ga droplets as catalyst [*53, 54*]. Because no native silicon oxides were removed beforehand, the Si substrate temperature was increased to 530°C, and one monolayer (ML) of Ga was deposited on the substrate at an equivalent GaAs two-dimensional growth rate of 0.50 ML/s [*55, 56*]. Then, the substrate temperature was increased to 610°C to begin the growth of GaAs NWs by providing Ga and As fluxes simultaneously. The GaAs growth rate was fixed at 0.75 ML/s with a beam equivalent pressure (BEP) of Ga and As_4 equal to 3.6 x 10^{-7} Torr and 3.6 x 10^{-6} Torr, respectively. During growth, the sample holder was continuously rotated to enhance the growth homogeneity. Two samples were fabricated: sample 1 (S1) was grown during 10 minutes, while sample 2 (S2) was grown during 100 minutes. As a result, S2 NWs are longer than S1 NWs but also thicker due

to radial overgrowth during the VLS axial growth. After the Ga shutter closure, the sample was cooled down to room temperature (RT) under an As_4 atmosphere to avoid GaAs decomposition. The As capping procedure was initiated after the substrate cooled down to RT following the growth of GaAs samples S1 and S2. For the As-capping of the obtained NWs, the temperature of the As cracking-cell was increased up to 950°C to supply As_2 instead of As_4. The samples were exposed to As_2 for about 2 hours. S1 was dedicated to the TEM experiments while S2 was dedicated to the SPEM/XPS measurements.

In situ TEM characterization

The TEM experiments have been performed in a FEI Titan ETEM G2, equipped with a spherical aberration corrector of the objective lens, a Gatan imaging filter (GIF) TRIDIEM for electron energy-loss spectroscopy measurements, and operated at 300 kV. The *in situ* annealing experiments were carried out using a dedicated Wildfire heating holder from DENSsolutions. NWs were transferred to a MEMS chip with a Si_3N_4 membrane by mechanically scrapping NWs off their native silicon substrate. The EELS elemental maps were obtained after background subtraction and integration of the Ga-L_{23} (~1120 eV) and As-L_{23} edges (~1330 eV) using the Digital Micrograph (Gatan Microscopy Suite) software.

Synchrotron radiation scanning photoelectron microscopy

X-ray photoemission experiments were performed at the nano-XPS endstation of the ANTARES beamline of the SOLEIL synchrotron (Paris, France), equipped with Fresnel zone plates for focalization of the synchrotron radiation beam, with a spot size of ~600 nm in this work. The experiments were carried out at a photon energy of 100 eV and linear horizontal light polarization, with an angular resolution of ~0.2º and an energy resolution of ~30 meV [57]. The sample was kept at room temperature and the base pressure during all experiments

was better than 2×10^{-10} mbar. The advantage of the nano-XPS technique for the study of NWs is that the X-ray beam spot size is small enough ensuring that the XPS measured is obtained in a particular area of a single few μm-long NW.

Associated content

The Supporting Information is available free of charge at

Figure S1: TEM bright field imaging and STEM-EELS elemental mapping of arsenic crystallization during shell decapping of sample S1.
Video V1: *in situ* TEM cristallization of the As shell.
Figure S2: Evolution of the NW diameter during *in situ* TEM annealing.
Table S1: Measured binding energy.
Figure S3: STEM-EELS analysis of a NW after decapping of the arsenic shell.

Author information

L.F., X.G., C.B., P.R. and M.G. synthesized the specimens. L.F., G.G., H.Y., J.A. and J.P. performed the SPM experiments and data analysis. L.F., M.B. and J.P. performed the *in situ* TEM experiments, and data analysis. M.B. and J.P. designed the study and wrote the manuscript. All authors contributed to the manuscript.

Corresponding Authors

Matthieu Bugnet – Univ Lyon, CNRS, INSA Lyon, UCBL, MATEIS, UMR 5510, 69621 Villeurbanne, France ; orcid.org/0000-0002-8272-8964 ;
Email : matthieu.bugnet@insa-lyon.fr

José Penuelas – Univ Lyon, Ecole Centrale de Lyon, CNRS, INSA Lyon, Université Claude Bernard Lyon 1, CPE Lyon, INL, UMR 5270, 69130 Ecully, France ;
orcid.org/0000-0002-5635-7346 ;
Email : jose.penuelas@ec-lyon.fr

Authors

Louise Fouquat – Univ Lyon, Ecole Centrale de Lyon, CNRS, INSA Lyon, Université Claude Bernard Lyon 1, CPE Lyon, INL, UMR 5270, 69130 Ecully, France
Xin Guan – Univ Lyon, Ecole Centrale de Lyon, CNRS, INSA Lyon, Université Claude Bernard Lyon 1, CPE Lyon, INL, UMR 5270, 69130 Ecully, France
Claude Botella – Univ Lyon, Ecole Centrale de Lyon, CNRS, INSA Lyon, Université Claude Bernard Lyon 1, CPE Lyon, INL, UMR 5270, 69130 Ecully, France
Geneviève Grenet – Univ Lyon, Ecole Centrale de Lyon, CNRS, INSA Lyon, Université Claude Bernard Lyon 1, CPE Lyon, INL, UMR 5270, 69130 Ecully, France
Philippe Regreny – Univ Lyon, Ecole Centrale de Lyon, CNRS, INSA Lyon, Université Claude Bernard Lyon 1, CPE Lyon, INL, UMR 5270, 69130 Ecully, France
Michel Gendry – Univ Lyon, Ecole Centrale de Lyon, CNRS, INSA Lyon, Université Claude Bernard Lyon 1, CPE Lyon, INL, UMR 5270, 69130 Ecully, France
Hemian Yi – ANTARES Beamline, Synchrotron SOLEIL & Université Paris-Saclay, L'Orme des Merisiers, Gif sur Yvette Cedex, France

José Avila – ANTARES Beamline, Synchrotron SOLEIL & Université Paris-Saclay, L'Orme des Merisiers, Gif sur Yvette Cedex, France

Notes

The authors declare no competing financial interest.

Acknowledgements

This work has been partly funded by the French Agence Nationale de la Recherche, project BEEP (ANR-18-CE05-0017-01). The Chinese Scholarship Council (CSC) is acknowledged for its financial support. The TEM work has been carried out at the consortium Lyon-St-Etienne de microscopie (CLYM). The authors thank the NanoLyon platform for access to equipment and J. B. Goure for technical assistance. SOLEIL is acknowledged for providing beamtime at the ANTARES beamline (proposal 20170235).

References

[**1**] Krogstrup, P., Jørgensen, H. I., Heiss, M., Demichel, O., Holm, J. V., Aagesen, M., ... & i Morral, A. F. Single-nanowire solar cells beyond the Shockley–Queisser limit. *Nature photonics* **2013**, *7*(4), 306-310.

[**2**] Zhang, Y., Wu, J., Aagesen, M., & Liu, H. III–V nanowires and nanowire optoelectronic devices. *Journal of Physics D: Applied Physics* **2015**, *48*(46), 463001.

[**3**] Kornienko, N., Gibson, N. A., Zhang, H., Eaton, S. W., Yu, Y., Aloni, S., ... & Yang, P. Growth and photoelectrochemical energy conversion of wurtzite indium phosphide nanowire arrays. *ACS nano* **2016**, *10*(5), 5525-5535.

[**4**] Vettori, M., Piazza, V., Cattoni, A., Scaccabarozzi, A., Patriarche, G., Regreny, P., ... & Gendry, M. Growth optimization and characterization of regular arrays of GaAs/AlGaAs core/shell nanowires for tandem solar cells on silicon. *Nanotechnology* **2018**, *30*(8), 084005.

[**5**] Vanka, S., Zhou, B., Awni, R. A., Song, Z., Chowdhury, F. A., Liu, X., ... & Mi, Z. InGaN/Si double-junction photocathode for unassisted solar water splitting. *ACS Energy Letters* **2020**, *5*(12), 3741-3751.

[**6**] Chuang, S., Gao, Q., Kapadia, R., Ford, A. C., Guo, J., & Javey, A. Ballistic InAs nanowire transistors. *Nano letters* **2013**, *13*(2), 555-558.

[**7**] Mårtensson, T., Svensson, C. P. T., Wacaser, B. A., Larsson, M. W., Seifert, W., Deppert, K., ... & Samuelson, L. Epitaxial III− V nanowires on silicon. *Nano letters* **2004**, *4*(10), 1987-1990.

[**8**] Huang, Y., Duan, X., & Lieber, C. M. Nanowires for integrated multicolor nanophotonics. *Small* **2005**, *1*(1), 142-147.

[**9**] Yan, R., Gargas, D., & Yang, P. Nanowire photonics. *Nature photonics* **2009**, *3*(10), 569-576.

[**10**] Hocevar, M., Immink, G., Verheijen, M., Akopian, N., Zwiller, V., Kouwenhoven, L., & Bakkers, E. Growth and optical properties of axial hybrid III–V/silicon nanowires. *Nature communications* **2012**, *3*(1), 1-6.

[**11**] Saxena, D., Mokkapati, S., Parkinson, P., Jiang, N., Gao, Q., Tan, H. H., & Jagadish, C. Optically pumped room-temperature GaAs nanowire lasers. *Nature photonics* **2013**, *7*(12), 963-968.

[**12**] Zhao, S., Woo, S. Y., Bugnet, M., Liu, X., Kang, J., Botton, G. A., & Mi, Z. Three-dimensional quantum confinement of charge carriers in self-organized AlGaN nanowires: A viable route to electrically injected deep ultraviolet lasers. *Nano letters* **2015**, *15*(12), 7801-7807.

[**13**] Ra, Y. H., Wang, R., Woo, S. Y., Djavid, M., Sadaf, S. M., Lee, J., ... & Mi, Z. Full-color single nanowire pixels for projection displays. *Nano Letters* **2016**, *16*(7), 4608-4615.

[**14**] Bermúdez-Ureña, E., Tutuncuoglu, G., Cuerda, J., Smith, C. L., Bravo-Abad, J., Bozhevolnyi, S. I., ... & Quidant, R. Plasmonic waveguide-integrated nanowire laser. *Nano letters* **2017**, *17*(2), 747-754.

[**15**] Liu, X., Le, B. H., Woo, S. Y., Zhao, S., Pofelski, A., Botton, G. A., & Mi, Z. Selective area epitaxy of AlGaN nanowire arrays across nearly the entire compositional range for deep ultraviolet photonics. *Optics express* **2017**, *25*(24), 30494-30502.

[**16**] Jaffal, A., Redjem, W., Regreny, P., Nguyen, H. S., Cueff, S., Letartre, X., ... & Chauvin, N. InAs quantum dot in a needlelike tapered InP nanowire: a telecom band single photon source monolithically grown on silicon. *Nanoscale* **2019**, *11*(45), 21847-21855.

[**17**] Vukajlovic-Plestina, J., Kim, W., Ghisalberti, L., Varnavides, G., Tütüncuoglu, G., Potts, H., ... & i Morral, A. F. Fundamental aspects to localize self-catalyzed III-V nanowires on silicon. *Nature communications* **2019**, *10*(1), 1-7.

[**18**] Hauge, H. I. T., Verheijen, M. A., Conesa-Boj, S., Etzelstorfer, T., Watzinger, M., Kriegner, D., ... & Bakkers, E. P. Hexagonal silicon realized. *Nano letters* **2015**, *15*(9), 5855-5860.

[**19**] Fadaly, E. M., Dijkstra, A., Suckert, J. R., Ziss, D., van Tilburg, M. A., Mao, C., ... & Bakkers, E. P. Direct-bandgap emission from hexagonal Ge and SiGe alloys. *Nature* **2020**, *580*(7802), 205-209.

[**20**] Mourik, V.; Zuo, K.; Frolov, S. M.; Plissard, S. R.; Bakkers, E. P. A. M.; Kouwenhoven, L. P. Science **2012**, *336*, 1003

[**21**] Krogstrup, P., Ziino, N. L. B., Chang, W., Albrecht, S. M., Madsen, M. H., Johnson, E., ... & Jespersen, T. S. Epitaxy of semiconductor–superconductor nanowires. *Nature materials* **2015**, *14*(4), 400-406.

[**22**] Hilse, M., Herfort, J., Jenichen, B., Trampert, A., Hanke, M., Schaaf, P., ... & Riechert, H. GaAs–Fe3Si core–shell nanowires: Nanobar magnets. *Nano letters* **2013**, *13*(12), 6203-6209.

[**23**] Guan, X., Becdelievre, J., Meunier, B., Benali, A., Saint-Girons, G., Bachelet, R., ... & Penuelas, J. GaAs core/SrTiO3 shell nanowires grown by molecular beam epitaxy. *Nano letters* **2016**, *16*(4), 2393-2399.

[**24**] Hjort, M., Lehmann, S., Knutsson, J., Timm, R., Jacobsson, D., Lundgren, E., ... & Mikkelsen, A. Direct imaging of atomic scale structure and electronic properties of GaAs wurtzite and zinc blende nanowire surfaces. *Nano letters* **2015**, *13*(9), 4492-4498.

[**25**] Hjort, M., Knutsson, J. V., Mandl, B., Deppert, K., Lundgren, E., Timm, R., & Mikkelsen, A. Surface morphology of Au-free grown nanowires after native oxide removal. *Nanoscale* **2015**, *7*(22), 9998-10004.

[**26**] Guan, X., Becdelievre, J., Benali, A., Botella, C., Grenet, G., Regreny, P., ... & Penuelas, J. GaAs nanowires with oxidation-proof arsenic capping for the growth of an epitaxial shell. *Nanoscale* **2016**, *8*(34), 15637-15644.

[**27**] Xu, T., Dick, K. A., Plissard, S., Nguyen, T. H., Makoudi, Y., Berthe, M., ... & Caroff, P. Faceting, composition and crystal phase evolution in III–V antimonide nanowire heterostructures revealed by combining microscopy techniques. *Nanotechnology* **2012**, *23*(9), 095702.

[**28**] Capiod, P., Xu, T., Nys, J. P., Berthe, M., Patriarche, G., Lymperakis, L., ... & Grandidier, B. Band offsets at zincblende-wurtzite GaAs nanowire sidewall surfaces. *Applied Physics Letters* **2013**, *103*(12), 122104.

[**29**] Díaz Álvarez, A., Xu, T., Tütüncüoglu, G., Demonchaux, T., Nys, J. P., Berthe, M., ... & Grandidier, B. Nonstoichiometric low-temperature grown GaAs nanowires. *Nano letters* **2015**, *15*(10), 6440-6445.

[**30**] Álvarez, A. D., Peric, N., Vergel, N. A. F., Nys, J. P., Berthe, M., Patriarche, G., ... & Grandidier, B. Importance of point defect reactions for the atomic-scale roughness of III–V nanowire sidewalls. *Nanotechnology* **2019**, *30*(32), 324002.

[**31**] Schnedler, M., Xu, T., Portz, V., Nys, J. P., Plissard, S. R., Berthe, M., ... & Grandidier, B. Composition modulation by twinning in InAsSb nanowires. *Nanotechnology* **2019**, *30*(32), 324005.

[**32**] Dursap, T., Vettori, M., Danescu, A., Botella, C., Regreny, P., Patriarche, G., ... & Penuelas, J. Crystal phase engineering of self-catalyzed GaAs nanowires using a RHEED diagram. *Nanoscale Advances* **2020**, *2*(5), 2127-2134.

[**33]** Jakob, J., Schroth, P., Feigl, L., Hauck, D., Pietsch, U., & Baumbach, T. Quantitative analysis of time-resolved RHEED during growth of vertical nanowires. *Nanoscale* **2020**, *12*(9), 5471-5482.

[**34**] Rudolph, D., Hertenberger, S., Bolte, S., Paosangthong, W., Spirkoska, D., Döblinger, M., ... & Koblmüller, G. Direct observation of a noncatalytic growth regime for GaAs nanowires. *Nano letters* **2011**, *11*(9), 3848-3854.

[**35**] Scarpellini, D., Fedorov, A., Somaschini, C., Frigeri, C., Bollani, M., Bietti, S., ... & Sanguinetti, S. Ga crystallization dynamics during annealing of self-assisted GaAs nanowires. *Nanotechnology* **2016**, *28*(4), 045605.

[**36**] Glas, F., Harmand, J. C., & Patriarche, G. Why does wurtzite form in nanowires of III-V zinc blende semiconductors?. *Physical Review Letters* **2007**, *99*(14), 146101.

[**37**] Krogstrup, P., Curiotto, S., Johnson, E., Aagesen, M., Nygård, J., & Chatain, D. Impact of the liquid phase shape on the structure of III-V nanowires. *Physical Review Letters* **2011**, *106*(12), 125505.

[**38**] Jacobsson, D., Panciera, F., Tersoff, J., Reuter, M. C., Lehmann, S., Hofmann, S., ... & Ross, F. M. Interface dynamics and crystal phase switching in GaAs nanowires. *Nature* **2016**, *531*(7594), 317-322.

[**39**] Dursap, T., Vettori, M., Botella, C., Regreny, P., Blanchard, N., Gendry, M., ... & Penuelas, J. Wurtzite phase control for self-assisted GaAs nanowires grown by molecular beam epitaxy. *Nanotechnology* **2021**, *32*(15), 155602.

[**40**] Avila, J., Razado-Colambo, I., Lorcy, S., Lagarde, B., Giorgetta, J. L., Polack, F., & Asensio, M. C. ANTARES, a scanning photoemission microscopy beamline at SOLEIL. In *Journal of Physics: Conference Series* **2013**, *425*(19), 192023.

[**41**] Jabeen, F., Rubini, S., Martelli, F., Franciosi, A., Kolmakov, A., Gregoratti, L., ... & Kiskinova, M. Contactless monitoring of the diameter-dependent conductivity of GaAs nanowires. *Nano Research* **2010**, *3*(10), 706-713.

[**42**] Zeller, P., Amati, M., Sezen, H., Scardamaglia, M., Struzzi, C., Bittencourt, C., ... & Gregoratti, L. Scanning photoelectron spectro-microscopy: a modern tool for the study of materials at the nanoscale. *Physica Status Solidi* 2018, *215*(19), 1800308.

[**43**] van Omme, J. T., Zakhozheva, M., Spruit, R. G., Sholkina, M., & Garza, H. H. P. Advanced microheater for in situ transmission electron microscopy; enabling unexplored analytical studies and extreme spatial stability. *Ultramicroscopy* **2018**, *192*, 14-20.

[**44**] Niekiel, F., Kraschewski, S. M., Müller, J., Butz, B., & Spiecker, E. Local temperature measurement in TEM by parallel beam electron diffraction. *Ultramicroscopy* **2017**, *176*, 161-169

[**45**] Šimečková, M., & Hrubý, A. A study on the crystallization of amorphous Arsenic. *Materials Research Bulletin* **1977**, *12*(1), 65-72.

[**46**] Fauske, V. T., Huh, J., Divitini, G., Dheeraj, D. L., Munshi, A. M., Ducati, C., ... & van Helvoort, A. T In situ heat-induced replacement of GaAs nanowires by Au. *Nano letters* **2016**, *16*(5), 3051-3057.

[**47**] Tornberg, M., Jacobsson, D., Persson, A. R., Wallenberg, R., Dick, K. A., & Kodambaka, S. Kinetics of Au–Ga droplet mediated decomposition of GaAs Nanowires. *Nano letters* **2019**, *19*(6), 3498-3504.

[**48**] Gott, J. A., Beanland, R., Fonseka, H. A., Peters, J. J., Zhang, Y., Liu, H., & Sanchez, A. M. Defect Dynamics in Self-Catalyzed III–V Semiconductor Nanowires. *Nano letters* **2019**, *19*(7), 4574-4580.

[**49**] Albe, K., Nordlund, K., Nord, J., & Kuronen, A. Modeling of compound semiconductors: Analytical bond-order potential for Ga, As, and GaAs. *Physical Review B* **2002**, *66*(3), 035205.

[**50**] Gang, G. W., Lee, J. H., Kim, S. Y., Jeong, T., Kim, K. B., Men, N. T. H., ... & Kim, Y. H. Microstructural evolution in self-catalyzed GaAs nanowires during in-situ TEM study. *Nanotechnology* **2021**, *32*(14), 145709.

[**51**] Choi, S., Lee, J., Pin, M., Kwon, J. H., Kim, I., Yeom, M. S., ... & Kim, Y. H. Anisotropic atomistic evolution during the sublimation of polar InAs nanowires. *Nanoscale* **2019**, *11*(14), 6685-6692.

[**52**] Vettori, M., Danescu, A., Guan, X., Regreny, P., Penuelas, J., & Gendry, M. Impact of the Ga flux incidence angle on the growth kinetics of self-assisted GaAs nanowires on Si (111). *Nanoscale Advances* **2019**, *1*(11), 4433-4441.

[**53**] Colombo, C., Spirkoska, D., Frimmer, M., Abstreiter, G., & i Morral, A. F. Ga-assisted catalyst-free growth mechanism of GaAs nanowires by molecular beam epitaxy. *Physical Review B* **2008**, *77*(15), 155326.

[**54**] Fontcuberta i Morral, A., Colombo, C., Abstreiter, G., Arbiol, J., & Morante, J. R. Nucleation mechanism of gallium-assisted molecular beam epitaxy growth of gallium arsenide nanowires. *Applied Physics Letters* **2008**, *92*(6), 063112.

[**55**] Tauchnitz, T., Nurmamytov, T., Hübner, R., Engler, M., Facsko, S., Schneider, H., ... & Dimakis, E. (2017). Decoupling the two roles of Ga droplets in the self-catalyzed growth of GaAs nanowires on SiO x/Si (111) substrates. *Crystal Growth & Design* **2017**, *17*(10), 5276-5282.

[**56**] Fouquat, L., Vettori, M., Botella, C., Benamrouche, A., Penuelas, J., & Grenet, G. X-ray photoelectron spectroscopy study of Ga nanodroplet on silica-terminated silicon surface for nanowire growth. *Journal of Crystal Growth* **2019**, *514*, 83-88.

[**57**] Avila, J.; Asensio, M. C. *Synchrotron Radiation News* **2014**, *27*, 24−30.

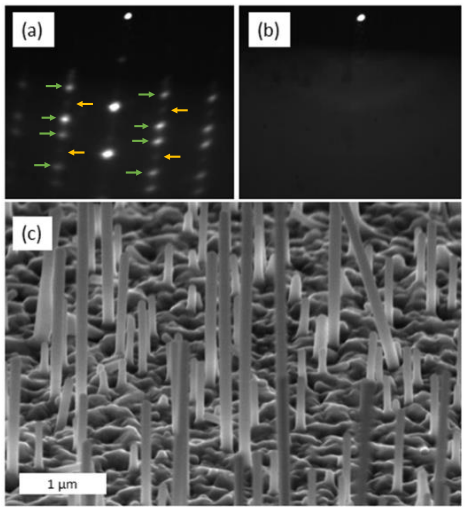

Figure 1. RHEED patterns (a) before the As capping, highlighting the presence of ZB (green arrows) and WZ phases (orange arrows), and (b) after the As capping. (c) SEM image of sample S1 after the growth.

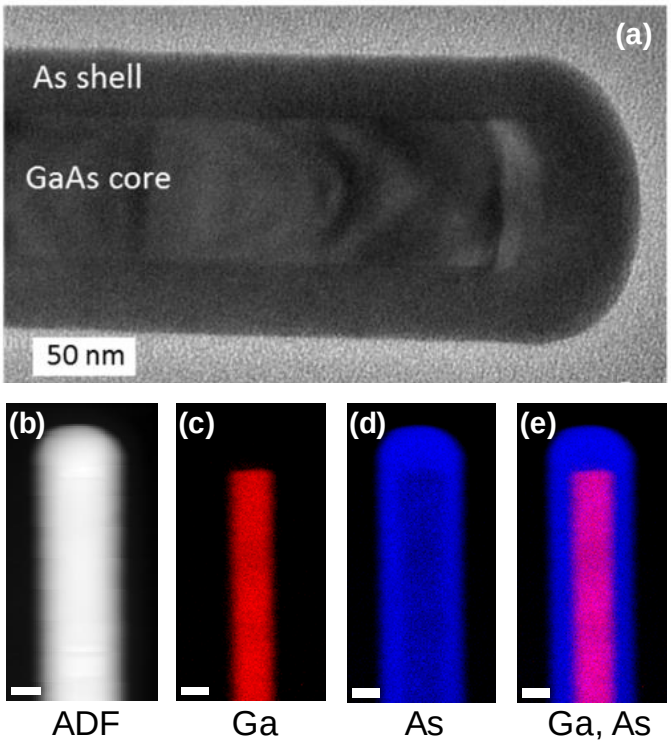

Figure 2. (a) Bright field TEM image of the as grown As/GaAs NW. (b) STEM-ADF image acquired simultaneously with a STEM-EELS spectrum image leading to the elemental maps of (c) Ga, (d) As, and (e) Ga+As. Scale bar: 50 nm

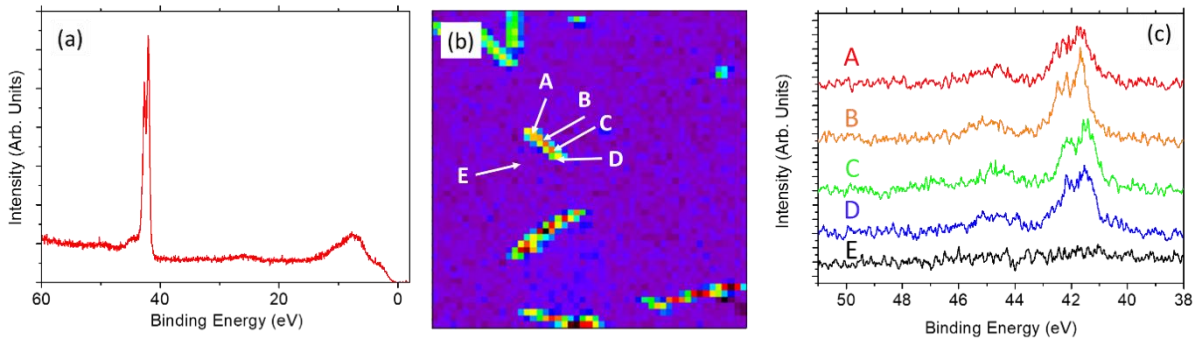

Figure 3. (a) XPS spectrum of sample S2 showing the region including As 3*d*, Ga 3*d* and valence band measured with a large spot size of 0.6 µm. (b) SPEM image (50×50 µm²) obtained with a pixel size of 400×400 nm² and filtered at a binding energy of 41.5 eV +- 1 eV corresponding to metallic As. (c) Five spectra (A, B, C, D) extracted from the map in (b) measured on a single nanowire, and a reference spectra (E) measured on the substrate. The photon energy was set to 100 eV.

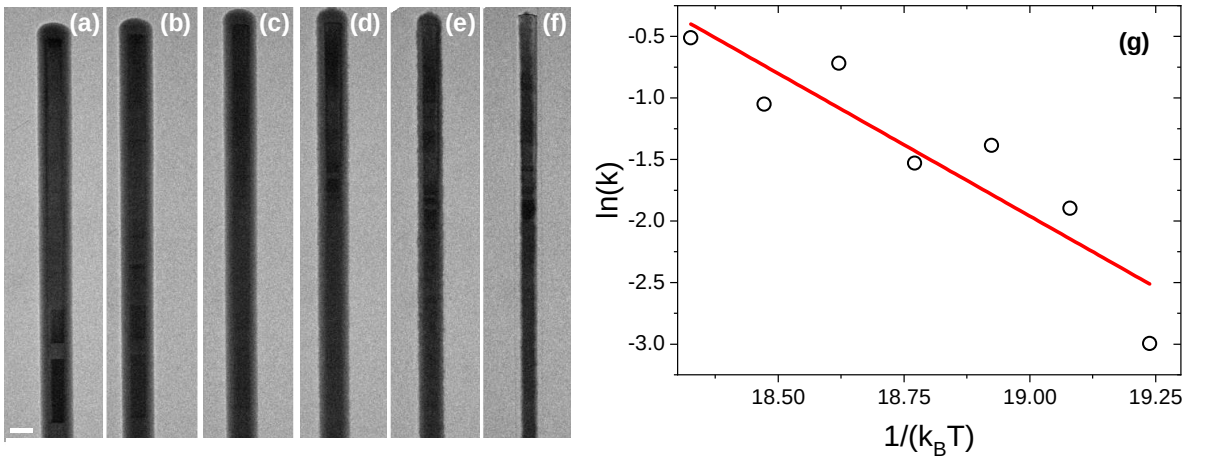

Figure 4. (a-f) Bright field TEM images of a single NW (sample S1) showing the desorption of the As shell, recorded at T = 300 ºC (a), 315 ºC (b), 330 ºC (c), 345 ºC (d), 360 ºC (e), 375 ºC (f). Scale bar: 100 nm. (g) Arrhenius plot extracted from the NW diameter evolution).

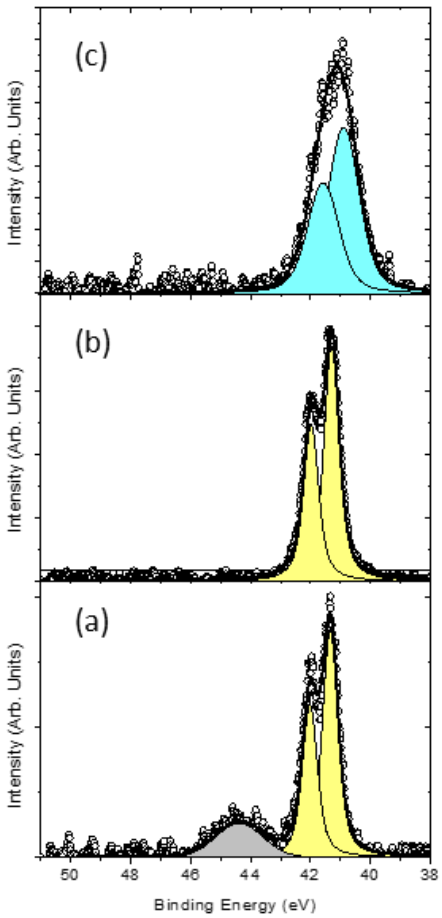

Figure 5. XPS As 3*d* core level spectra measured on a typical NW before annealing (a), after the first annealing at 400°C (b), after the second annealing at 440°C (c). The photon energy was set to 100 eV. The grey curve corresponds to As oxide, the yellow curve to metallic As and the blue curve to As in GaAs.

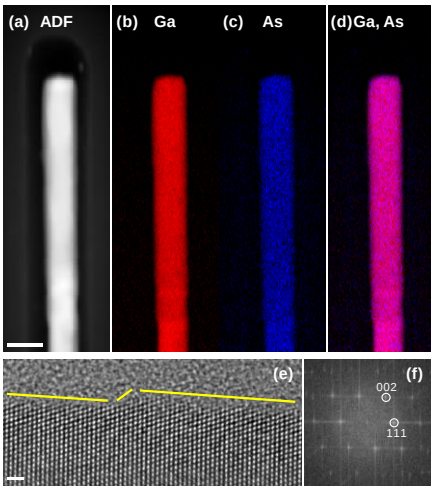

Figure 6. (a) STEM-ADF image acquired simultaneously with an EELS spectrum image leading to the elemental maps of (b) Ga, (c) As, and (d) Ga+As; scale bar: 100 nm. (e) High resolution TEM image of the NW after decapping of the As shell; scale bar: 1 nm. The yellow lines follow the facets and are guides for the eye. (f) FFT performed on the NW shown in (e).

For Table of Contents Only